

## Observing With a CCD

## Camera Properties and Measuring Brightness and Position

**Purpose**

The purpose of this lab was to gain experience both in taking data with the direct-imaging CCD system on the 0.5 m telescope and in analyzing the resulting images on the astrolab computer using VNC and IDL. Most of the data analysis for this lab involved using the RUPhAst image display tool to display and examine images.

The lab also determined important properties of the CCD system. The separation of pairs of stars in M39 yielded the image scale. The combination of images of the inside of the dome with nearly uniform illumination and zero-length (bias) images yielded important properties of the CCD camera: the gain and read noise.

**I. Preparation and Planning**

1. Both M39 and 230 Athamantis were high in sky during our lab periods. If the first group of the night took their calibration data first, both objects would be higher in the sky later. But neither was uncomfortably low at 7:00 PM, so the order of observing did not matter much. Both M39 and Athamantis crossed the meridian slightly before 10:00 PM, and so the second group did have enough time to get set up and take data before the crossing, though they could avoid any time pressure if they waited until the second half of their session.
2. Zooming into M39 in *The Sky* showed that all of the stars labeled in the finding chart would fit in the field of view of the CCD camera. I found it helpful to turn off the thumbnail picture of the cluster and just display the stars in the database of *The Sky*, since this makes those stars “clickable”. This is done with the “Non-Stellar Options” in the View menu. The brighter stars in the cluster itself are suitable for focusing.
3. There was always a 7<sup>th</sup> – 8<sup>th</sup> magnitude star within a few degrees of Athamantis for focusing, and usually there was a star well-placed for guiding – though sometimes the star was fainter than is ideal (such was the case for the pair of images that I made available to the class).

**II & III. Observations of M39, Athamantis, and Calibration Data**

The poor weather at the beginning of the semester continued during this lab, so no groups were able to obtain guided images of M39 (90 seconds long) and Athamantis (10 seconds produced a well-exposed image of the asteroid, though in hindsight 90 seconds would have been better). All but the Tuesday night groups had obtained flat-field and bias images using the inside of the dome.

I supplied the class with an image of M39 taken at 02:07:47 UT on 30 September 2017 (so 10:07 PM EDT on the 29<sup>th</sup>). I believe that the sky was clear when it was taken. I also made available two images of Athmantis that I had taken on UT September 30, 2018 (i.e., on the evening of September 29). The file headers give the UT of the first image as 03:42:08.056 and of the

second as 03:57:28.458. The images were guided, though the guide star was faint – about 10.6. Since the asteroid was high in the sky and the weather was clear, this was bright enough with a 6 second exposure on the guider.

#### IV. Data Analysis Part 1: Visual Observing vs. CCD imaging

Part of the image of M39 is shown in Figure 1 below with an inverted color map (much preferable when printing) and rotated counter-clockwise by 90 degrees. This image has the same orientation as the top finding chart from Lab 2.

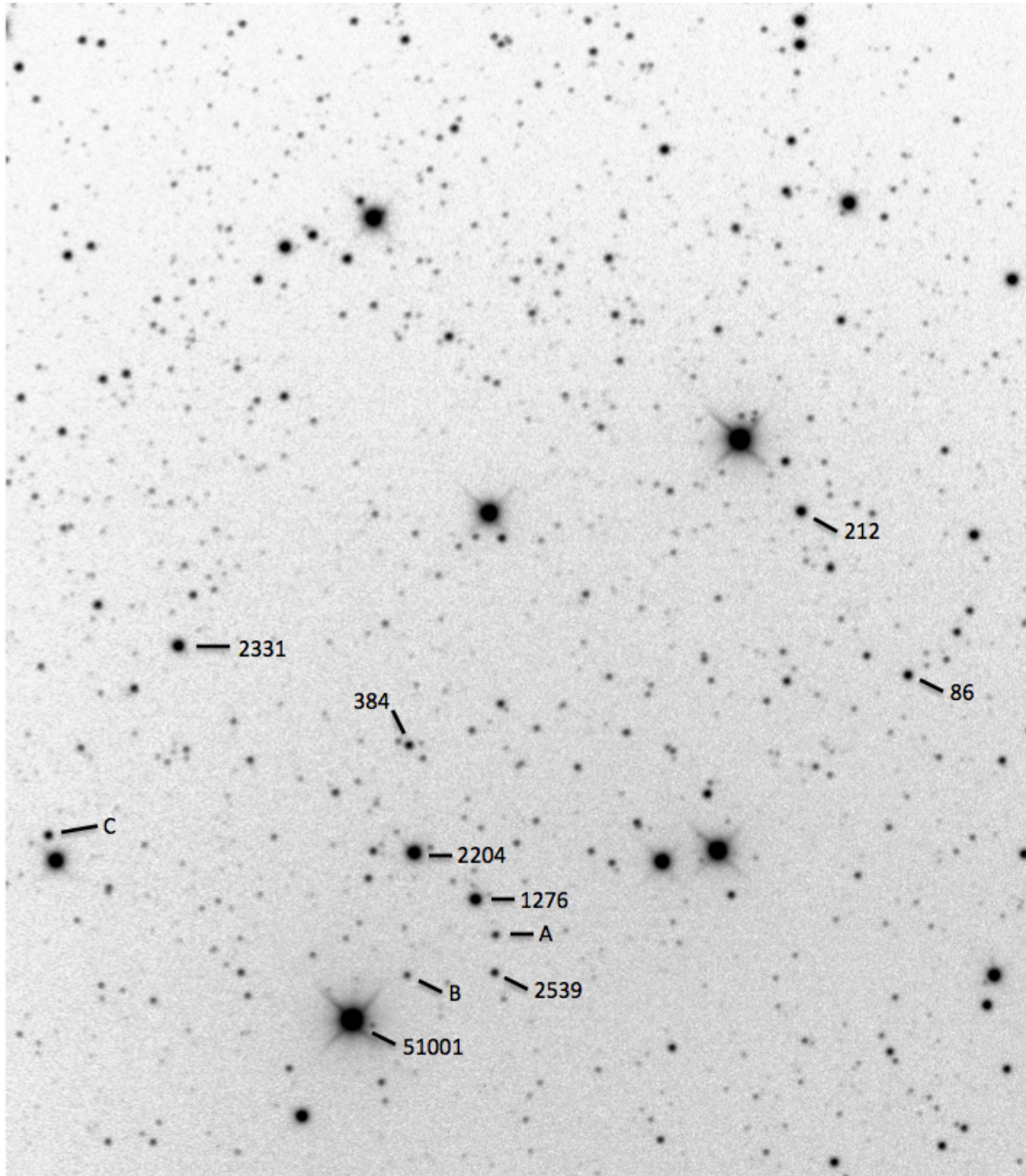


Figure 1. A portion of a 90-second exposure of M39. North is up and east to the left.

Matching the stars in the image and the finding chart shows that even the faintest two stars on the list, TP A and TP B (with magnitudes of 13.6 and 14.0, respectively), are visible in the 90-s exposure. No one was able to see these two stars visually (well, one person thought that they might have glimpsed TP A). The visibility of the faint stars in the CCD image probably owes primarily to its longer integration time compared to the eye (90 s vs. 1/30<sup>th</sup> s). Using magnitudes from various sources (including color-magnitude diagrams produced for this class in previous years), the faintest stars visible in the image have a magnitude of about 16.7.

## V. Data Analysis Part 2: Image Scale

I used the p-key in *RUPhAst* to measured the positions, (x,y), of all five of the stars listed in the lab write-up in the M34 exposure described earlier. For the small angular separations within our image, it is a very good approximation to calculate the angular separation,  $s$ , between two stars with right ascension and declination ( $\alpha_1, \delta_1$ ) and ( $\alpha_2, \delta_2$ ) using  $\Delta\alpha = (\alpha_2 - \alpha_1)\cos((\delta_1 + \delta_2)/2)$ ,  $\Delta\delta = \delta_2 - \delta_1$ , and  $s = ((\Delta\alpha)^2 + (\Delta\delta)^2)^{1/2}$ . Note that it is much simpler to convert the right ascension and declination from the given sexagesimal notation into decimal degrees, as discussed in class. The table below gives ( $\Delta\alpha, \Delta\delta$ ) in arcseconds and ( $\Delta x, \Delta y$ ) in pixels measured from the first star, GSC 3594:86.

Table 1. Position Data and Image Scale for M39

Star	$\Delta\alpha$ (arcsec)	$\Delta\delta$ (arcsec)	$s$ (arcsec)	$x$ (pixels)	$y$ (pixels)	$\Delta x$ (pixels)	$\Delta y$ (pixels)	$s$ (pixels)	Scale ("/pixel)
86				1331.9	239.3				
384	438.60	-57.75	442.38	1262.7	731.8	-69.2	492.5	497.3	0.88951
2331	640.47	31.01	641.22	1360.8	959.7	28.9	720.4	721.0	0.88938
2539	365.24	-258.07	447.21	1038.3	647.2	-293.6	407.9	502.6	0.88984
TP C	756.28	-134.73	768.19	1173.8	1088.2	-158.1	848.9	863.5	0.88963

Dividing the separation between a pair of stars,  $s$ , in arcseconds by the separation in pixels gives the four estimates of the image scale in Table 1. They are approximately independent, though not completely so since all of the estimates have one star (and the errors in its measured position) in common. Averaging them yields 0.88959 arcsec/pixel with a root-mean-square scatter around this mean of 0.00017 arcsec/pixel. Taking the scatter as an estimate of the uncertainty in individual estimate, the uncertainty in the mean is smaller by  $1/\sqrt{4}$  or 0.00008 arcsec/pixel. Averaging the image scales yielded by all ten possible pairs of the five stars yields a scale of 0.88969 arcsec/pixel. If the root-mean-square scatter of the ten values around their mean is taken as the estimate of the uncertainty in a single measurement and it is assumed that there are still only four independent measurements, then the uncertainty of the mean is 0.00014 arcsec/pixel. The difference between 0.88959 arcsec/pixel and 0.88969 arcsec/pixel could be noise, though it could also reflect a not-unexpected variation of the image scale with position in the image. Measuring many more stars would be required to decide between the two possibilities.

A more effective way to use all of the information in the stellar positions is to fit for the coefficients in the transformation:

$$\Delta\alpha = S(-\Delta x \sin \theta + \Delta y \cos \theta)$$

$$\Delta\delta = S(\Delta x \cos \theta + \Delta y \sin \theta).$$

This transformation is a rotation and scale change and defines  $\theta = 0$  such that declination increases along x and right ascension increases along y (which is close to being true). Such a simple form is often adequate, though it is only an approximation: we are projecting a sphere onto a plane and the telescope and camera optics can introduce distortions of their own. A few in the class took a step in this direction by calculating the image scale separately for the x and y directions and then averaging. Using least squares to find the best-fitting coefficients yields  $S = 0.88957$  arcsec/pixel and  $\theta = 0.47$  degrees. So the x-axis is very close to being aligned along the north-south line and the y-axis along east-west. A similar transformation using coordinates instead of offsets can produce  $(\alpha, \delta)$  from  $(x,y)$ .

## VI. Data Calibration Part 1: CCD Gain and Read Noise

### Random Numbers and Statistics

This part of the lab consisted of starting idlde and issuing the IDL commands that generate an array of random numbers. Technically these numbers are only “pseudo-random” numbers since computers are designed to always give the same results for the same inputs. Anyone interested in pursuing the subject of random numbers generated by computers is referred to the relevant chapter in Volume II, *Seminumerical Algorithms*, of Knuth’s *The Art of Computer Programming*.

2. A two-dimensional array of Gaussian random numbers with zero mean and unit standard deviation produces a speckled image that averages to a uniform gray (see the image in Figure 2 below). Zooming in makes the individual darker and brighter pixels visible.

3 & 4. The image statistics for each random realization of the Gaussian distribution will be slightly different, but should be very similar to these:

For  $11 \times 11$  box:

Minimum pixel value:	-2.525
Maximum pixel value:	+2.173
Mean:	-0.0737
Median:	-0.1037
Standard Deviation:	1.0198

For  $151 \times 151$  pixel box:

Minimum pixel value:	-4.125
Maximum pixel value:	+3.886
Mean:	-0.00092
Median:	-0.00221
Standard Deviation:	1.00141

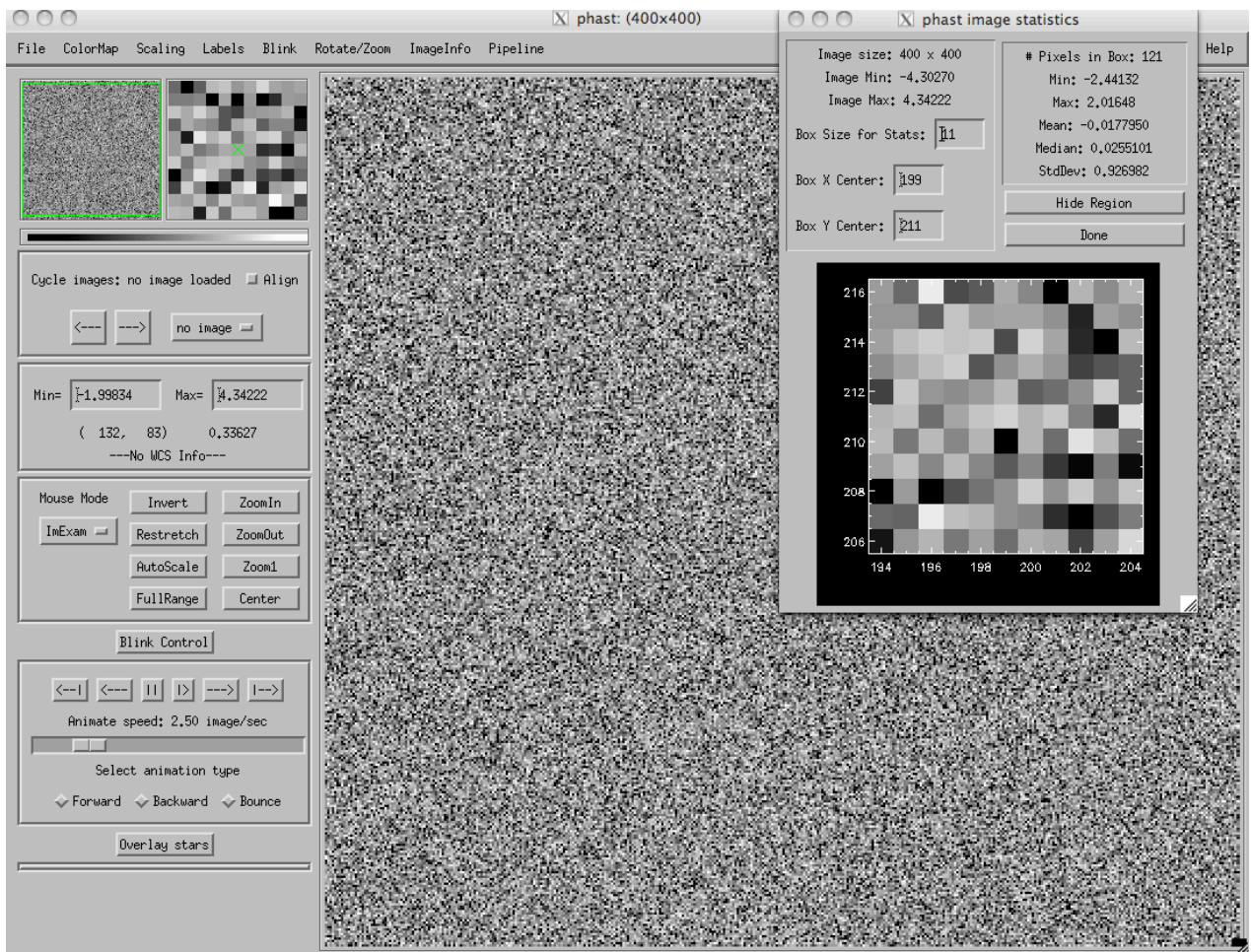


Figure 2. *RuPhAst* display of an image of Gaussian random pixel values.

Since each box has only a finite number of random values drawn from a Gaussian distribution, you do not expect the mean to be exactly zero and the standard deviation to be exactly one. For example, the expected standard deviation of the mean of  $N$  values is the standard deviation expected for a single value divided by the square root of  $N$  (*i.e.*, this is the expected scatter of many such estimates of the mean around the true mean). For the above two samples this is:

$$11 \times 11 \text{ box (121 samples):}$$

$$\text{S.D. of mean} = 1.0198 / (121)^{1/2} = 0.0927$$

$$151 \times 151 \text{ box (22,801 samples):}$$

$$\text{S.D. of mean} = 1.00141 / (22801)^{1/2} = 0.0066$$

Note that the means and medians differ from 0.000 by amounts comparable to these expectations in each case. Of course, it is always possible by chance to have a mean that is closer to zero than expected (or somewhat, though not a lot, more distant). A few students in the class did have the

mean of the smaller sample to be closer to zero than that of the larger sample for this reason (or the standard deviation to be closer to one), often to their surprise.

In general, as the sample size gets larger, the precision of statistical estimators such as the mean, standard deviation, *etc.* gets better. Also, note that in the larger samples the maximum and minimum values get farther from zero, since there is a greater chance of seeing the rare large fluctuations.

### Gain and Read Noise of Low-Gain Mode

7. Image Structure: The image headers contain a variety of useful data. Quantities that are particularly relevant to this lab are the binning, the size of the image read out, the exposure time, and the commanded and measured CCD temperature. Quantities that are important for observations of the celestial objects are the (commanded) filter, the date and time of the observation, and the right ascension and declination at which the telescope was pointing. (The image header currently does not contain the right ascension and declination towards which the computer thinks the telescope is pointing. *The Sky* and *CCDSOFT* are supposed to communicate to pass this information, but this is not happening due to the increased restrictions placed on inter-process communication in more recent versions of the Windows operating system.)

A 2×2-binned bias image is shown below in Figure 3 with a non-inverted color map. The image size is 2004 pixels horizontally by 1336 pixels vertically (4008×2672 pixels for no binning). There are no overscan pixels in either direction. The exposure time was of 0 seconds and the CCD temperature was −15.2 C. A few individual bright pixels and columns are apparent, produced by pixels with much higher than average dark current (“hot pixels”). The major feature visible is a vertical gradient, caused by dark current in the vertical transfer registers. The readout time is approximately 16 seconds in total, or about 12 msec per row of the CCD. The bottom row is read out immediately, so it has essentially 0 seconds total exposure time to accumulate dark current. Each successive row has about 12 msec of additional time to accumulate dark current, so the image gets brighter towards the top. The uppermost row accumulates dark current for the entire readout time, making its total exposure time about 16 seconds.



Figure 3. A  $2 \times 2$ -binned bias image.

A plot of the central column of the image clearly shows this linearly increasing dark current:

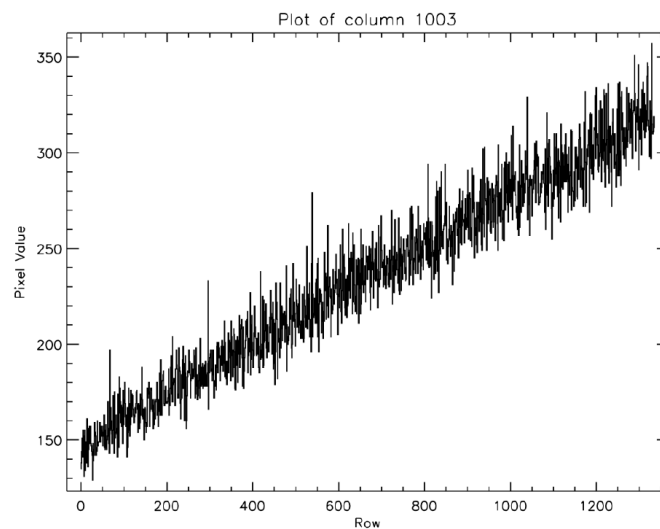


Figure 4. Plot of the signal values in column 1003 of the bias image shown in Figure 3.

In these  $2 \times 2$ -binned (low-gain) images, the bias level (the electronic offset applied before the signal is digitized) is about 150 ADU, as seen in Figure 4 above. The dark signal accumulated at the end of the readout is about 170 ADU ( $320 - 150$ ), so the dark current at this temperature in

the transfer region is 10.6 ADU/sec. Using the manufacturer's gain specification of 1.62  $e^-$ /ADU, this is a dark current of 6.6  $e^-$ /sec per binned pixel or 1.6  $e^-$ /sec per unbinned pixel.

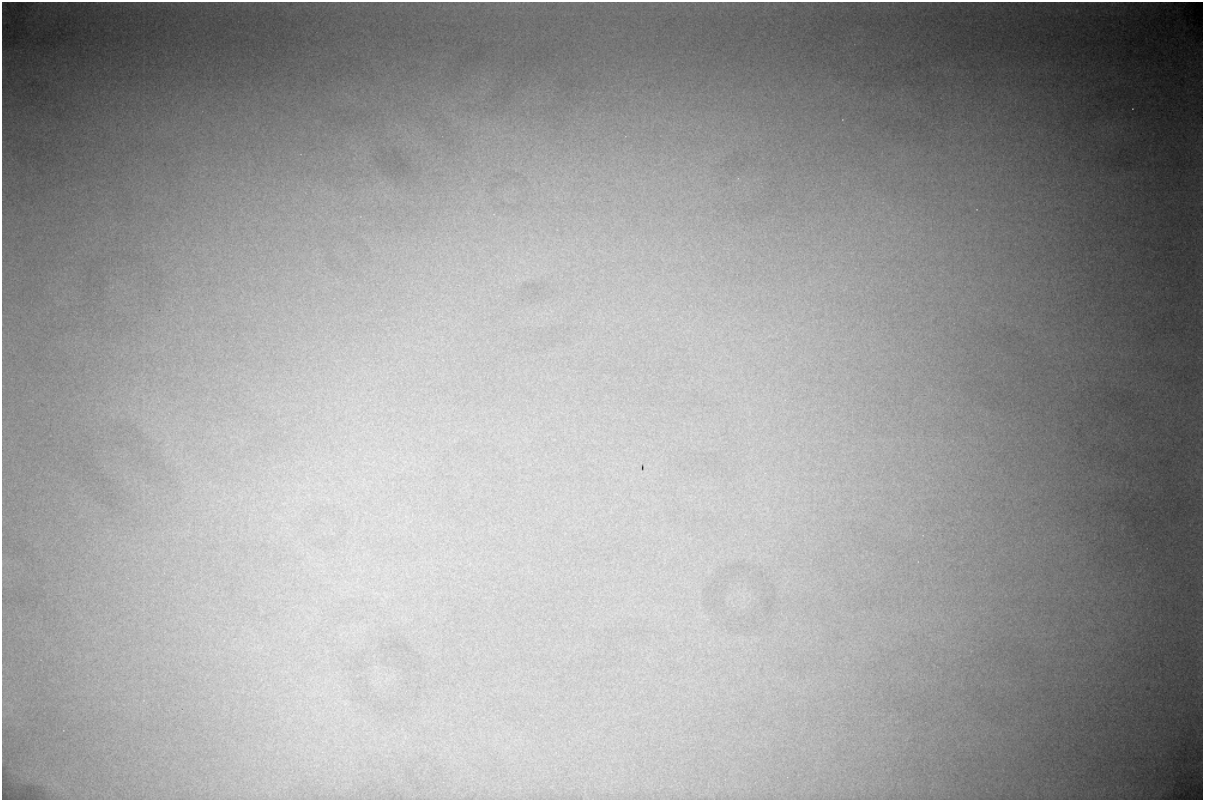


Figure 5. A 2×2-binned flat-field image taken with the V filter.

A 2×2-binned, V-band “flat-field” image produced by observing the inside of the dome is shown above with a non-inverted color map. The exposure time was 7.5 seconds. There is a gradient in the illumination of about 10% over the image, caused by vignetting in the camera optics (causing the dark corners of the image) and, perhaps, by the dome not being uniformly illuminated. In addition to the defect pixels and columns that were also visible in the bias image, there are several fuzzy donut-shaped structures – these are out-of-focus images caused by dust on the CCD window, the filter, and/or the fold mirror that directs light into the CCD.

#### 5. – 11. Gain and Read Noise

Note that the *CCDSOft* program saves the fits images by default as unsigned 16-bit integers; this preserves the full dynamic range of the CCD data system for each image, but the unsigned representation and limited bit depth rapidly lead to problems when you begin to do arithmetic on the images. The simple way to fix this in IDL is to convert the images to 32-bit floating point representation by multiplying each image by the constant 1.0 after it is read in. Following the analysis procedure described in the lab gives the values included in Tables 2 and 3 below. Although the lab only asked you to measure the statistics at a single location in each image (a  $51 \times 51$  box centered in the image), I calculated the statistics in five non-overlapping boxes near the bottom of the image. In boxes near the bottom of the image, the dark current is least and so the spurious contribution of the noise in the dark current to the estimate of the read noise is minimized. Though it could be argued that, since the dark

current cannot be eliminated, it is more realistic to include its effect and so obtain an “effective read noise.” Five measurements of the gain and read noise allow an estimate of their uncertainties based on how well the different values agree.

Table 2. Low Gain Measurements

X,Y	200, 50		400, 50		500, 50		600, 50		800, 50	
	mean	st dev	mean	st dev	mean	st dev	mean	st dev	mean	st dev
b1	168.174	10.4310	166.404	10.7072	165.904	10.3993	166.364	11.2946	165.972	10.9938
b2	167.988	10.6075	166.780	10.7867	165.629	10.5567	166.320	11.0602	165.878	11.0856
db	0.186	12.2669	-0.376	12.1867	0.275	12.2054	0.044	12.1752	0.094	12.5523
f1	41993.6	201.081	42671.5	203.521	42832.8	202.075	42881.5	196.619	42929.3	198.628
f2	41997.4	205.835	42658.4	201.738	42829.1	200.201	42872.4	198.089	42929.5	197.655
df	-3.9	215.098	13.1	219.527	3.7	217.441	9.2	221.268	-0.3	218.654
gain	1.808 e/ADU		1.763 e/ADU		1.805 e/ADU		1.745e/ADU		1.789 e/ADU	
noise	15.68 e		15.20 e		15.58 e		15.02 e		15.88 e	

If only random Gaussian read noise were producing the standard deviation around the mean for the bias images, then the standard deviation of the difference of two biases should be larger than that of one frame by the  $\sqrt{2}$ . The standard deviation of the difference is actually somewhat smaller than that, suggesting that pixel-to-pixel differences in the dark current or bias level are contributing to the scatter around the mean in the  $51 \times 51$  pixel box for individual images. Taking the difference between two images eliminates this source of variation, leaving just the read noise. Similarly, the standard deviation around the mean of the difference of two flat-field images is much less than  $\sqrt{2}$  times the standard deviation for the individual images. Pixel-to-pixel gain differences and non-uniform illumination contribute to the standard deviation for an individual image – the difference of two images just has the scatter due to photon statistics. Estimating the gain and read noise using two boxes near the top of the image yields very similar values for the gain, 1.788 and 1.831 e<sup>-</sup>/ADU, but larger read noises, 20.68 and 21.12 e<sup>-</sup>.

Table 3. High Gain Measurements

X,Y	200, 50		400, 50		500, 50		600, 50		800,50	
	mean	stdev								
b1	682.514	14.5977	681.306	14.5900	681.500	14.6064	680.752	13.8166	681.802	14.0885
b2	682.825	14.6500	681.383	14.3629	682.728	14.6171	682.287	14.0081	681.887	13.9472
db	-0.311	18.0115	-0.077	17.9945	-1.228	17.9999	-1.535	18.3392	-0.086	18.2990
f1	43208.2	300.936	43195.2	305.802	43235.6	307.525	43234.3	305.359	43177.4	304.847
f2	43210.0	303.205	43203.5	303.184	43226.7	301.837	43223.7	306.044	43186.0	308.452
df	-1.7	315.017	-8.2	308.959	8.9	308.864	10.6	317.086	-8.6	314.817
gain	0.857 e/ADU		0.890 e/ADU		0.892 e/ADU		0.846 e/ADU		0.858 e/ADU	
noise	10.92 e		11.34 e		11.35 e		10.98 e		11.10 e	

Though not required by the lab, Table 3 above gives similar results for pairs of high-gain ( $1\times 1$  binning) flats and biases. The behavior of the standard deviations is the same as for the low-gain data. The read noise estimated using boxes near the top of the image was about  $13.6 e^-$ .

The average gains and read noises from the five locations in the two sets of images are:

Table 4. Average Gain and Read Noise

	High Gain	Low Gain
Gain (e/ADU)	$0.8688 \pm 0.0095$	$1.782 \pm 0.012$
Read Noise (e)	$11.136 \pm 0.090$	$15.47 \pm 0.16$

The CCD system vendor quotes the gains in the two modes as 1.62 and 0.81 e/ADU, respectively, and a *typical* read noise of 11 electrons RMS. Our measurements are in reasonable agreement with these values. Note the confusing terminology associated with the “gain” of a CCD system. A high amplifier gain in the system means that fewer electrons are needed to produce a digital unit (ADU), resulting in a lower “gain” (really an inverse gain) in  $e^-/\text{ADU}$ . The low-gain read noise is significantly greater than the high-gain read noise. One would expect the read noise, in electrons, to be the same in the two gain modes. The significantly larger noise in low-gain mode suggests that there is a significant contribution to the total system noise after the amplification stages, possibly in the bias offset that is applied before the signal is digitized. For comparison, a good (and expensive) professional-grade CCD system has a read noise of about 3 electrons per pixel.

## VII. Analysis: Identify Athamantis and Measure its Motion

Because no groups were able to obtain images for this lab, I supplied two that I had taken on UT September 30, 2018 (i.e., on the evening of September 29). The file headers give the UT of the first image as 03:42:08.056 and of the second as 03:57:28.458. Blinking between the pair of auto-guided images makes Athamantis immediately stand out as the only “star” that moves. I measured the locations of Athmantis and six stars in the pair of images obtained for the lab. The stars are similar in brightness to the asteroid and spread across the image. I used the “centroid” algorithm in the aperture photometry tool instead of the “snap to” algorithm (I think that the latter finds the location of the maximum signal), as it seemed to give more accurate positions. The data are given in Table 5 below, which lists the location in the two images,  $(x,y)$ , and its change between the images,  $(\Delta x, \Delta y)$  in pixels, for each object. The agreement between the positions of the stars at the two times argues that the uncertainty in the positions is about  $\pm 0.1$  pixel. Presumably this applies to the positions of Athamantis as well. Sometimes students use the measured full-width at half maximum (FWHM) of the images, about 5 pixels, as an estimate of the uncertainty in each coordinate of the position. This is too pessimistic – it is generally possible to measure the center of an image of a star to a fraction of the FWHM. A useful rule-of-thumb is that the uncertainty is the FWHM divided by the signal-to-noise of the image. Our images of Athamantis had  $S/N \approx 190$ , implying an uncertainty in the measured positions of about 0.03 pixel in the  $x$  and  $y$  directions. This is apparently too optimistic for these data, possibly because of the simple

estimate of the position used by *RUPhAst*. The more sophisticated methods that I use in my research can approach the above level of accuracy.

The positions of the stars in Table 5 also indicate that the two auto-guided images are offset from one another by  $-0.03 \pm 0.05$  pixels in  $x$  and  $-0.30 \pm 0.02$  pixels in  $y$ . The offset in  $y$  is statistically significant. Where these offsets come from is unclear to me, though blinking between the images does show somewhat different shapes for the stellar images in the two images. It is possible that these changes are due to somewhat different guiding errors or seeing fluctuations between the two images. However, last year I saw similar offsets (up to 0.5 pixel) in 90-second exposures of a different asteroid and I would have thought that a 90 s exposure would average over errors in guiding to produce smaller offsets than that (and, in any case, smaller offsets than for a 10-second exposure). It could be that we are seeing the effect of small changes in the focus, though 10 minutes does not allow much time for such a change to occur.

Table 5. Measurement of the Angular Speed of 230 Athamantis

Object	$x_1$	$y_1$	$x_2$	$y_2$	$\Delta x$	$\Delta y$	$\Delta S$ (pixels)	$\Delta t$ (min)	Speed (arcsec/hr)	Corr. Speed
Athamantis	679.5	726.3	674.6	724.1	-4.9	-2.2	5.37	15.34	18.7	18.2
Star 1	730.5	254.6	730.6	254.3	0.1	-0.3	0.32			
Star 2	1386.1	705.1	1386.0	704.8	-0.1	-0.3	0.32			
Star 3	1135.8	450.6	1135.6	450.3	-0.2	-0.3	0.36			
Star 4	434.4	512.3	434.5	512.0	0.1	-0.3	0.32			
Star 5	1504.0	910.2	1504.0	910.0	0.0	-0.2	0.20			
Star 6	619.5	1169.3	619.4	1168.9	-0.1	-0.4	0.41			

The times of the images are recorded to the nearest 0.001 s. It is unlikely that the computer clock is in synchrony with Universal Time at that level, but it likely is able to measure an interval of about 10 minutes with about that level of precision. In any case, it is clear that the accuracy of the measured speed of the asteroid is determined by the accuracy of the measured positions for the asteroid and not the times of the images. The motion of Athamantis between the two exposures is  $\Delta S = ((\Delta x)^2 + (\Delta y)^2)^{1/2}$ . The uncertainty in this quantity is given by the propagation of errors:

$$\sigma_{\Delta S} = \left( \left( \frac{\partial \Delta S}{\partial \Delta x} \sigma_{\Delta x} \right)^2 + \left( \frac{\partial \Delta S}{\partial \Delta y} \sigma_{\Delta y} \right)^2 \right)^{1/2} = \left( \left( \frac{\Delta x}{\Delta S} \sigma_{\Delta x} \right)^2 + \left( \frac{\Delta y}{\Delta S} \sigma_{\Delta y} \right)^2 \right)^{1/2} \approx \sigma_{\Delta x, y}.$$

The last step in the above assumes that  $\sigma_{\Delta x} = \sigma_{\Delta y} = \sigma_{\Delta x, y}$ . Multiplying  $\Delta S$  by the pixel scale (0.8897 arcsec/pixel), dividing by  $\Delta t$ , and multiplying by 60 to convert to arcseconds per hour yields the speed of 18.7 arcsec/hour listed in the next-to-last column of the table. If  $\sigma_{\Delta x, y} = 0.1$  pixel, then the uncertainty in the asteroid speed is  $\pm 0.3$  arcsec/hr. There is also potentially a contribution to the uncertainty in the measured speed from the uncertainty in the

image scale. If  $v_p$  is the speed in pixel/hr,  $v$  is the speed in arcsec/hr, and  $I$  is the image scale, then  $v=Iv_p$  and propagation of errors gives

$$\sigma_v = \left| \frac{\partial v}{\partial I} \right| \sigma_I = v_p \sigma_I = v \left( \frac{\sigma_I}{I} \right).$$

My measurement of the image scale has  $\sigma_I/I = 0.0001/0.8896 = 0.0001$ , implying an uncertainty in  $v$  from this source of about 0.02 arcsec/hr. Since the uncertainties from the two sources add in quadrature, the contribution from uncertainty in the image scale is negligible. This was not the case for those who found a larger uncertainty in the image scale.

The images of Athamantis were taken west of the meridian, so the positive  $x$  direction is north and the positive  $y$  direction is east. Thus, the direction of motion was approximately south-southwest. Taking an arctangent yields the position angle (measured from north through east) for the velocity vector on the sky of  $204 \pm 1$  degrees, where the uncertainty comes from the propagation of the uncertainties in  $\Delta x$  and  $\Delta y$ . Athamantis may have been in retrograde motion but was mostly moving towards the ecliptic (it was about 30 degrees north of the ecliptic when we observed it).

The shifts between the pairs of images of stars shown in Table 5 could introduce larger errors than the uncertainties discussed above. Subtracting the average  $\Delta x$  and  $\Delta y$  for the six stars from those for Athamantis produces the corrected speed of 18.2 arcsec/hr in the last column of Table 5. The corrected position angle of the motion is  $200 \pm 1$  degrees.

The above speed and direction of motion are in reasonable agreement with those given by an ephemeris for Athamantis from the International Astronomical Union Minor Planet Center (<http://www.minorplanetcenter.net/iau/MPEph/MPEph.html>). The ephemeris shows that the speed of the asteroid at 04<sup>h</sup> on 30 September 2018 was 18.36 arcsec/hr with a position angle for the velocity vector of 197.6 degrees.